IOP Publishing Plasma Phys. Control. Fusion 68 (2026) 085014 https://doi.org/10.1088/1361-6587/ae8b28

Plasma Physics and Controlled Fusion



RECEIVED
27 January 2026

REVISED
7 May 2026

ACCEPTED FOR PUBLICATION
15 July 2026

PUBLISHED
7 August 2026



PAPER

# Fast evaluation of the Fast-Ion $D_\alpha$ spectroscopy measurements at the ASDEX Upgrade tokamak

B Tosto[1,*], M Weiland[2], M Cavedon[1], A Kappatou[2], D Kulla[2] and the ASDEX Upgrade Team[3]

[1] Department of Physics Giuseppe Occhialini, University of Milano-Bicocca, Milan, Italy
[2] Max-Planck Institute for Plasma Physics, Garching, Germany
[3] See Pütterich *et al* 2026 (https://dx.doi.org/10.1088/1741-4326/ae61c8) for ASDEX Upgrade Team.
[*] Author to whom any correspondence should be addressed.

**E-mail:** b.tosto@campus.unimib.it

**Keywords:** spectroscopy, fast ions, FIDA, fast analysis, look-up table

## Abstract

At the ASDEX Upgrade tokamak, a new fast method for the evaluation of the Fast-Ion $D_\alpha$ (FIDA) diagnostic has been developed. Up to now, the analysis of FIDA data required forward-modelling with the FIDASIM code, whose long calculation times restricted the analysis to single time points within a discharge. We developed a faster forward model, which makes it possible to study the evolution of the fast-ion distribution over whole discharges. The computational time to evaluate a single time point has been reduced from minutes to near real-time. The new method allows the reproduction of the FIDA spectrum using the FIDASIM weight functions approach: the spectral intensity is obtained by convolving the fast-ion distribution function with a weight function. The latter can be seen as the product between a wavelength-independent FIDA intensity function, called $R$, and an analytic probability of emission in a determined $\lambda$ range. The computational times are strongly reduced by adopting a look-up table (LUT), in which the $R$ functions computed by FIDASIM are stored as a function of the most relevant plasma parameters, line of sight geometry and neutral components (beam components and halo). The LUT requires the previous knowledge of the neutral densities inside the tokamak, for this purpose, a fast model has been implemented within the RABBIT code. A detailed evaluation of the new method's approximations is provided, highlighting the discrepancies identified relative to the FIDASIM reference.

## 1. Introduction

Fusion reactors will rely on fusion-born $\alpha$ particles for plasma heating. In current devices, without Deuterium-Tritium operation, supra-thermal ion populations are created by external heating systems, such as the neutral beam injection (NBI) and the ion cyclotron resonance heating (ICRH). Understanding the behaviour and ensuring an effective confinement of the fast ions is, therefore, crucial for efficient reactor operation.

Fast Ion $D_\alpha$ (FIDA) spectroscopy is a widely employed diagnostic used for fast ion studies in several machines [1–4]. It is based on the charge-exchange reaction between fast ions and neutrals:

$$D^+_{\text{fast}} + D^0 \rightarrow D^{0*}_{\text{fast}} + D^+. \tag{1}$$

Equation (1) holds for a $D$ beam and a $D$ plasma. The donor neutral $D^0$ can be both a fast neutral injected by the NBI, either at full, half or one third of the injection energy, or a thermal halo neutral. Since the reaction can be considered elastic, the fast ion $D^+_{\text{fast}}$ has the same velocity vector as the fast neutral $D^{0*}_{\text{fast}}$. The latter almost immediately de-excites, giving rise to a well localized radiation. FIDA looks at the Balmer-$\alpha$ line emission, the brightest falling in the visible range, at roughly 656.1 nm. The Einstein coefficient associated to the $3 \rightarrow 2$ transition is $A_{32} \approx 4.4 \times 10^7 \text{s}^{-1}$, corresponding to a characteristic emission timescale of $\approx 2.3 \times 10^{-8}$ s (data taken from [5]). When measuring the $D_\alpha$ spectrum, the FIDA emission can be clearly distinguished from the other spectral $D_\alpha$ components by its large

Doppler shift. Although easy to identify, the FIDA spectrum is difficult to interpret because energy and pitch can not be independently inferred from the wavelength shift. In addition, the radiance is proportional to the density of the fast ions that are neutralized along the line of sight (LOS), which involves the calculation of energy-dependent cross sections. Ultimately, the fast-ion distribution can not be determined from a single FIDA measurement, as only part of the distribution is sampled. For this reason, the data analysis is conventionally carried out with the FIDASIM code [6, 7]. Synthetic FIDA signals from a given fast-ion distribution are forward-modelled and, in this way, it can be assessed if the simulated fast-ion distribution matches with the experimental results. The standard forward modelling is based on a Monte Carlo simulation, while an alternative is represented by the weight function method (cf section 2). Due to the long computational times (on the order of minutes per simulation), FIDASIM allows to analyse only single time points within a discharge.

In this work, a fast analysis method based on the weight function approach is implemented. The reduced computational time allows the reproduction of the FIDA emission over entire discharges. This improvement enables the identification of time points of interest and the analysis of a large number of discharges, thereby supporting the creation of large databases. The new fast method also paves the way to future real-time applications.

Alternatively to FIDASIM's forward modelling approach, the fast-ion distribution function can be reconstructed by velocity-space tomography, using the information coming from different viewing directions [8, 9]. Tomography also relies on weight functions and therefore our new fast method could potentially make tomographic reconstructions faster and more widely available.

The weight function approach used to reproduce the FIDA intensity is described in section 2. In section 3, the concept of the new fast method is introduced. Detailed information on the implementation and verification of the look-up table (LUT) built to reproduce the weight functions is given in section 4. In section 5, the analytic formula to obtain the wavelength dependent emission probability is discussed. The fast neutral model implemented within RABBIT can be found in section 6. The verification of the new fast method is presented and discussed in section 7. Last, in section 8, the summary of the work is reported, along with the outlook.

## 2. The weight function approach

Weight functions represent the probability that a fast-ion of a specific energy and pitch range is neutralized and, subsequently, emits $D_\alpha$ radiation in a given wavelength range. Each wavelength bin $\Delta\lambda$ of the spectrum can be interpreted as the weighted integral over energy and pitch of the fast-ion distribution function:

$$I_{\mathrm{FIDA}}\left(\lambda_1,\lambda_2\right) = \frac{10^4}{4\pi\ \mathrm{d}\lambda}\int_{\infty}^{+\infty}\int_{-1}^{+1} W(\lambda_1,\lambda_2,E,p)\times F(E,p)\,\mathrm{d}E\mathrm{d}p \tag{2}$$

$W(\lambda_1,\lambda_2,E,p)$ is the weight function in [ph cm s$^{-1}$], $F(E,p)$ is the fast-ion distribution in [fast ions/(dE dp cm$^3$)], $\lambda_1$ and $\lambda_2$ are the limits of the chosen wavelength range, $E$ is the energy and $p$ is the pitch ($p = v_{||}/v$). $I_{\mathrm{FIDA}}$ is then obtained in [ph/(s nm m$^2$ sr)].

Weight functions depend on the geometry of the lines of sight, on the density of neutrals, on the kinetic plasma profiles and on the magnetic field vectors. Since the neutral density is concentrated around the neutral beam and the lines of sight are designed to go through it tangentially to flux surfaces, the FIDA radiation can be assumed to be well localized. Therefore, the conventional weight function approach neglects all spatial dependencies and the calculation uses the LOS integrated neutral densities and the LOS averaged plasma parameters weighted over the neutral density. Both these quantities, although involving the integral and the average over the whole LOS, can be considered almost local due to the strong concentration of the neutrals along the beam. This represents an approximation and small variations from the standard FIDASIM Monte Carlo approach, which is based on a 3D grid, are expected. The limitations that arise by ignoring the spatial dependencies can be overcome by augmenting the weight functions from 2D to 3D [10]. In this work, we accept this approximation and use the traditional 2D approach for the sake of simplicity. However, this introduces inaccuracies when the fast-ion distribution changes rapidly within the measurement volume. The weight function calculation also involves the solution of the collisional radiative model (evaluated spatially independently for the averaged plasma parameters) and the Doppler and Stark effects.

We note that, given its underlying assumptions, the weight function approach is formulated for active FIDA signals.

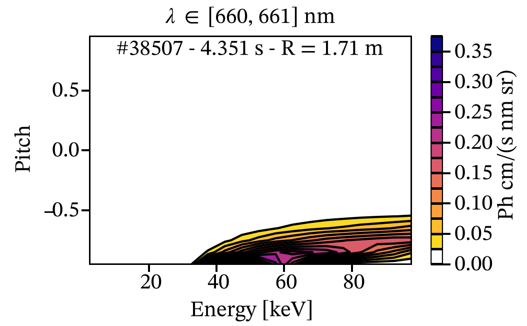


**Figure 1.** Weight function calculated with FIDASIM in the $\lambda$ range [660, 661] nm for a specific line of sight (toroidal) and time point. Each wavelength bin $\Delta\lambda$ of the spectrum has a different weight function. Examples of different weight function shapes can be found in [4, 11].

An example of a weight function calculated in the wavelength range [660, 661] nm for a specific LOS and time point of the discharge #38507 of ASDEX Upgrade is reported in figure 1. The shape of the weight function strongly depends on the $\lambda$ range considered. By calculating $I_{FIDA}(\lambda_1, \lambda_2)$ with weight functions in different wavelength ranges $\Delta\lambda$, the whole synthetic spectrum can be reconstructed.

## 3. Concept of the fast method

The basic idea of the new fast method is that the FIDA intensity can be obtained with reduced computational time if weight functions are obtained more efficiently, i.e. without performing the full FIDASIM calculation, assuming prior knowledge of a predicted fast-ion distribution (equation (2)). For this purpose, according to the derivation made in [11], we split the weight function calculation as follows:

$$W(\lambda_1, \lambda_2, E, p, \phi) = R(E, p)\,\mathrm{prob}(\lambda_1 < \lambda < \lambda_2 | E, p, \phi) \tag{3}$$

$R(E, p)$ is a $\lambda$-independent FIDA intensity function, which can be interpreted as $W(0, +\infty, E, p, \phi)$, i.e. a weight function integrated over all wavelengths. This quantity does not have an analytical expression but is instead implicitly computed within FIDASIM weight function calculation. It represents a line integrated flux of photons and constitutes an intermediate result obtained before to the inclusion of Doppler and Stark effects, which introduce the wavelength dependence. An example of $R$ function for each one of the four neutral components of #38507 is shown in figure 2: (a) full energy component, (b) half energy component, (c) one third energy component and (d) halo neutrals. Note that $R(E, p)$ has an implicit dependency on the overall geometry, so it changes for each LOS. Indeed, the calculation strongly depends on the line integrated neutral densities, line averaged plasma parameters and fields as well as on the time a fast ion takes to traverse the beam and halo neutral populations.

$\mathrm{prob}(\lambda_1 < \lambda < \lambda_2 | E, p, \phi)$ is the probability that a photon is emitted in a determined wavelength range, given the (E, p) coordinates and the projection angle $\phi$ between the LOS and the magnetic field. The latter probability can be calculated exploiting an analytical formula derived in [11], which is addressed in a subsequent step of the work and explained in greater detail in section 5.

Since no analytical equation is available to get the $R$ functions, we decide to reproduce them through a LUT, built within FIDASIM. For building the LUT, a further splitting is applied to equation (3):

$$W(\lambda_1, \lambda_2, E, p, \phi) = \frac{R(E, p)}{n_{\mathrm{LOS-int}}} \cdot n_{\mathrm{LOS-int}} \cdot \mathrm{prob}(\lambda_1 < \lambda < \lambda_2 | E, p, \phi) \tag{4}$$

with $n_{\mathrm{LOS-int}}$ the line-integrated neutral density. The ratio $R(E, p)/n_{\mathrm{LOS-int}}$, hereafter denoted $\tilde{R}$, is the quantity stored in the LUT. Since $R$ is proportional to the line integrated density, this normalization yields a density independent quantity suitable for analysing arbitrary discharges using the LUT. $\tilde{R}$ is therefore later multiplied by the actual line integrated density of the discharge under analysis. In FIDASIM, the neutral densities are calculated up to the energy level $n = 6$, so the neutral density by which the $R$ function is divided is given by the sum of the populations in the six levels. Even though $\tilde{R}$ is density independent, the dependency on the LOS geometry is still present.

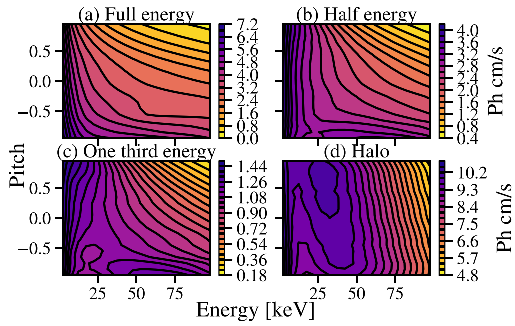


**Figure 2.** $R$ functions relative to #38507 at 4.351 s and $R = 1.71$ m. (a) full energy component, (b) half energy component, (c) one third energy component and (d) halo neutrals. The $R$ functions represent a line integrated flux of photons, an intermediate step to get the weight functions, still not related to the emission wavelength. By multiplying the $R$ function by the probability of the emission in a determined $\lambda$ range, the corresponding weight function is obtained. The $R$ functions are, therefore, a common factor for the calculation of the emission in every wavelength range.

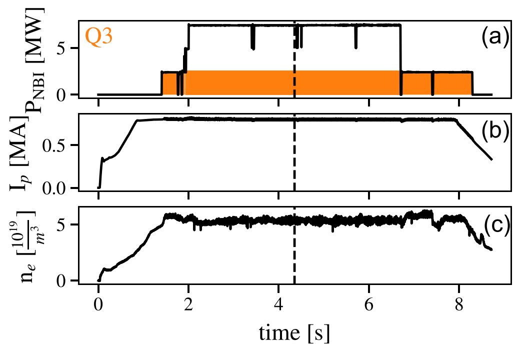


**Figure 3.** Time traces of #38507 related to (a) NBI power, (b) plasma current and (c) electron density. The time point used to build the look-up table is marked with a vertical dashed line. The NBI source relevant for the FIDA diagnostic is Q3 from box 1, highlighted in orange, the other active sources belong to box 2.

A further step consists in analysing the four neutral components (full, half and one third energy component and halo) separately. Given their different nature, an individual analysis permits to identify different behaviours and different parameters dependencies.

To build the LUT, a shot which features standard global parameters at a time point belonging to the flattop phase is selected. The shot is #38507 and the time point is 4.351 s, for which a good agreement between FIDASIM and the experimental measurements is obtained [12]. The main discharge parameters are displayed in figure 3: (a) NBI power, (b) plasma current, (c) electron density.

The evaluations that have to be done after this assumption are: how well will a LUT built on a reference shot work for different discharges? How much is the geometry of the LOS affecting the results, i.e. for shots from different experimental campaigns? All these open questions will be addressed in the following.

The new method in its entirety is outlined in the flowchart in figure 4. First, we need a simulated fast-ion distribution function. Here, in principle, any code can be used, from slower codes such as TRANSP, to real-time capable codes like RABBIT [13]. Within the new method, RABBIT is also used for a fast simulation of the neutral populations, from which the line integrated neutral densities and the line averaged plasma parameters are calculated. These are then used to obtain the $R$ function using the LUT. By means of an analytical formula for prob$(\lambda_1 < \lambda < \lambda_2 | E, p, \phi)$, the weight function can be reconstructed using equation (4). As a last step, the emission intensity can be easily obtained with equation (2).

To test the performance of the fast weight function calculation against FIDASIM, the fast-ion distribution simulated by TRANSP is used, i.e. the same one employed within FIDASIM. Future work will focus on interfacing the distribution function obtained from RABBIT with the new fast method, enabling the fast calculation of synthetic FIDA signals for entire discharges, potentially even in real-time.

In the next sections, all the different steps outlined in the flowchart will be described in detail, paying particular attention to the approximations introduced. The impact of the latter will always

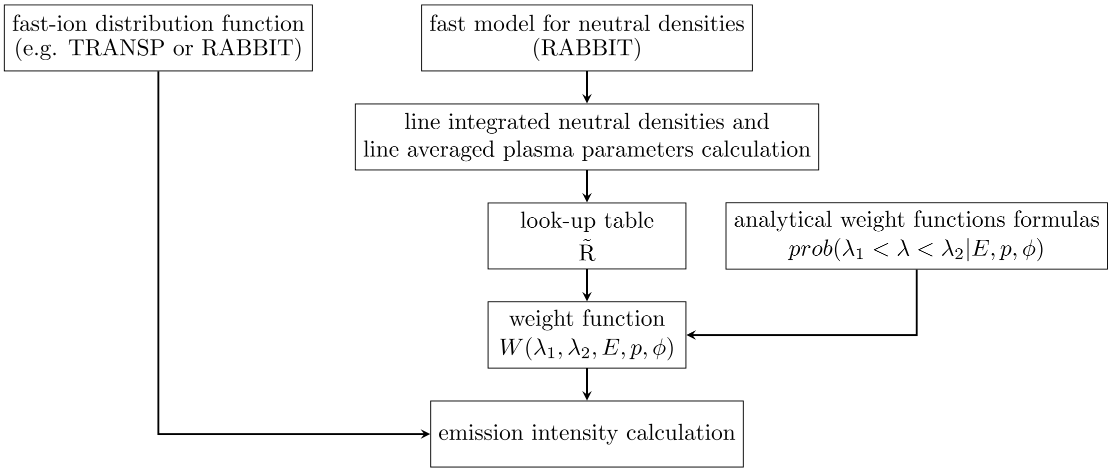


**Figure 4.** Flowchart summarizing the main steps in which the work is divided. A simulation code will be used to obtain the predicted fast-ion distribution (e.g. TRANSP or RABBIT). The RABBIT code will be used to calculate the line integrated neutral densities and the line averaged plasma parameters. The latter will be the inputs to obtain the $R$ function of the analysed shot by means of a look-up table. To obtain the weight function associated to a chosen wavelength range, the $R$ function will be multiplied by the probability of the emission in that range. With the knowledge of the weight function, the intensity of the $D_\alpha$ emission can be calculated with equation (2).

be assessed on the FIDA emission intensity (always against FIDASIM), since the final goal of the fast method is the evaluation of the spectrum.

We set as target to keep the relative error between the new method and FIDASIM approximately within 10%. Ideally, the smaller error, the better the performance. However, since the final goal is to reproduce the experimental spectrum, we also need to account for the impact of the approximations of the weight function method, as well as the non-negligible uncertainties in the experimental intensity calibration.

As a final remark, we recall that the adoption of the weight function approach in the new method implies that only active FIDA signals are considered. However, passive FIDA radiation is typically negligible, as edge neutral density and fast-ion profiles do not significantly overlap [14]. In cases where passive contributions are non-negligible, they can be subtracted from the experimental data before comparison with the new method.

## 4. The LUT for $\tilde{R}$

The LUT is the core of the new fast method. First, the implementation and the design are described in detail, then the performance is tested and assessed.

### 4.1. Sensitivity study

To build a LUT for the $\tilde{R}$ functions, their main dependencies need to be identified. The fundamental parameters on which the weight function calculation is based on are the line integrated neutral densities and the line averaged plasma parameters. Note that the line average is weighted over the neutral density ($k_{\mathrm{mean}} = \int k d_{\mathrm{j}}\, \mathrm{d}l / \int d_{\mathrm{j}}\, \mathrm{d}l$ with $k$ plasma parameter and $j = E$, $E/2$, $E/3$, halo). $\tilde{R}$ is by construction independent of the neutral density (equation (4)), therefore the most relevant parameters to consider are the line averaged plasma parameters. To assess which of them are affecting the calculation significantly, a sensitivity study is performed running FIDASIM and scaling the whole profile of each plasma parameter at a time. The profiles are both decreased and increased by multiplying by 0.5 and 1.5, respectively. The plasma parameters showing stronger variations are added to the dimensions of the LUT. Consistently with the assumptions made in section 3, the sensitivity study is performed on each neutral component separately. Given the different nature of the beam and halo neutrals, they can feature different plasma parameters dependencies and have different entries in the LUT.

The sensitivity study is performed on: electron density ($n_{\mathrm{e}}$), electron temperature ($T_{\mathrm{e}}$), ion temperature ($T_{\mathrm{i}}$), effective charge ($Z_{\mathrm{eff}}$) and plasma toroidal rotation ($v_{\mathrm{t}}$). The plots showing the complete results can be found in appendix A, while the outcome is summarized in the following:

**Table 1.** table summarizing the structure of the beam and halo neutrals look-up tables. The parameters included in each table are listed along with the respective ranges. The LUT's structure is chosen by searching for a balance between accuracy, computational time and storage size.

| | | | | | | | |
|---|---|---|---|---|---|---|---|
| NBI table<br>halo table | $E$ | $p$ | LOS | $n_e$ [cm$^{-3}$]<br>[1–10] $\times 10^{13}$ | $Z_{\mathrm{eff}}$<br>[1.2–2] | $T_e$ [keV]<br>[0.1–10] | $E_{\mathrm{inj}}$<br>$T_i$ [keV] [0.1–10] |

- $n_e$: parameter whose variation affects more the $R$ functions (15%–30%), no particular differences in the behaviour of the beam and halo neutrals are observed.
- $Z_{\mathrm{eff}}$: second parameter leading to noticeable variations in the $R$ functions (5%–16%). All the neutral components show the same percentage of agreement between the reference and the modified $R$ function for each LOS.
- $T_e$: parameter affecting in a slightly different way each neutral component, impacting more on the halo neutrals (1%–4%).
- $T_i$: as $T_e$, influences more the halo neutrals (again 1%–4%), while can be considered almost negligible for the beam neutrals, showing variations below 2% for each LOS.
- $v_t$: parameter showing a percentage of variation always below 2%, with a stronger impact, again, on the halo neutrals. This can be understood because the latter, differently from the beam neutrals, are a thermal population whose velocity vectors can be described by a Maxwell distribution shifted by plasma rotation.

All the results obtained are in agreement with the sensitivity study performed in section 4.3 of [15].

In conclusion, in the LUTs for both beam and halo neutrals are included $n_e$, $Z_{\mathrm{eff}}$ and $T_e$. The LUT for the halo neutrals will, in addition, include $T_i$.

### 4.2. Implementation and design

The LUT calculation is implemented within the FIDASIM code. Specifically, two different LUTs are made, with a slightly different design (summarized in table 1):

- Beam neutrals LUT: seven dimensional table that includes the $\tilde{R}$ functions for each one of the three velocity components of the neutral beam. The dimensions are: $E$, $p$, LOS, $n_e$, $Z_{\mathrm{eff}}$, $T_e$ and injection energy ($E_{\mathrm{inj}}$). The latter is set to the three different injection energies of the neutral components. Setting this parameter to one specific value, the $\tilde{R}$ function of the corresponding component is obtained, i.e. full, half or one third energy component.
- Halo neutrals LUT: seven dimensional table whose dimensions are $E$, $p$, LOS, $n_e$, $Z_{\mathrm{eff}}$, $T_e$ and $T_i$.

We recall that the LUT needs an entry for each LOS due to the already mentioned implicit dependency of the $\tilde{R}$ functions on the LOS. Although $\tilde{R}$ is defined to be independent of the neutral densities, with all plasma parameter dependencies incorporated into the LUT, it still contains the dependencies on the line averaged fields values and on the time fast ions spend traversing the beam and halo neutral populations.

The $\tilde{R}$ functions are stored for a grid of line integrated plasma parameters. The grid points are chosen to cover the whole range of possible values obtainable during a discharge in AUG. The number of points for each line integrated plasma parameter is chosen based on the sensitivity study: for the parameters with a stronger influence on the $R$ functions are selected ten points, while for the others only five. This choice is made to reduce the size of the table and, consequently, the computational times. The construction of one single LUT with this design requires up to half a day. The ranges chosen are: $n_e$ in [1–10]$\times 10^{13}$ cm$^{-3}$, $Z_{\mathrm{eff}}$ in [1.2–2] and $T_e$ and $T_i$ in [0.1–10] keV. The parameters for which ten points are set are electron density and effective charge. Concerning both electron and ion temperature, the points on the grid are not equidistant, but a finer tuning is used for lower temperatures. This is because the chosen range is wide enough to also cover discharges with high temperatures, although these are expected to remain well below 10 keV.

To summarize, the routine implemented within FIDASIM produces as output a LUT for the $\tilde{R}$ function, as a function of energy and pitch, associated to each neutral component, for each LOS and for each point on a grid of line integrated plasma parameters. To reproduce the $\tilde{R}$ function of an arbitrary shot using the LUT, after fixing the desired LOS, a four dimensional interpolation on the parameter grid is performed, using as target the already known LOS averaged plasma parameters of the new pulse. Since the calculation is strongly related to the geometry of the tokamak, the LUT can be used to analyse only shots of the same tokamak as the reference shot, in this case ASDEX Upgrade. Despite this, a LUT for another machine is straightforwardly obtained exploiting the same routine and using a different geometry as input, i.e. using a standard reference shot from another tokamak.

### 4.3. Verification

To check the approximations introduced, the FIDA emission intensities of different shots are calculated both with FIDASIM (using the weight function method) and the LUT and compared to each other. The comparison is made calculating the relative error on the LUT intensity as follows: $(I_{\mathrm{FIDASIM}} - I_{\mathrm{LUT}})/I_{\mathrm{FIDASIM}}$.

To obtain $\mathrm{I}_{\mathrm{LUT}}$, the interpolated $\tilde{R}$ from the LUT is first multiplied by the line integrated neutral density of the specific discharge. The resulting $R$ function is then multiplied by the probability of the emission in the selected wavelength range (equation (3)). Since the calculation of this probability constitutes a subsequent step of the new method, the LUT is, for initial verification, built using the weight functions instead of the $\tilde{R}$ functions. This approach allows the impact of the approximations introduced only by the LUT on the intensity calculation to be assessed. The wavelength range chosen is [660, 661] nm.

The tests are made for three different AUG discharges. First, to evaluate the approximations related only to the choice of the line integrated plasma parameters, the intensity of the reference shot (#38507) is calculated. Then, to assess how well the weight function of an arbitrary shot is reproduced using the LUT, two different discharges are selected. The first one belongs to the same experimental campaign as the reference shot, the second to a different one. This choice allows to estimate how much a relatively small displacement in the position of the lines of sight influences the results.

The comparison between the intensities computed with FIDASIM and the LUT will be shown only for the toroidal lines of sight (CER) of ASDEX Upgrade. To explain this choice, it must be recalled that the new method is based on the weight functions approach, which is an approximate method relying on the assumption that the FIDA radiation is well localized. The final target is to reproduce the experimentally observed emission intensity. If the FIDA radiation is not sufficiently localized along the LOS, the weight function calculation can lead to noticeable discrepancies with both the Monte Carlo and the observed spectrum. This is because it relies on line integrated and on line averaged quantities. According to [4], at ASDEX Upgrade the toroidal lines of sight provide the best radial resolution, as they are the most tangential to flux surfaces. For this reason, the verification of each step and of the new fast method will be shown only for those LOS. For the sake of completeness, the results for all the lines of sight are reported in appendix B.

The outcome of the comparison between the intensities computed with FIDASIM and the LUT for the three different shots is shown in figure 5 and summarized in the following:

(i) *Reference shot (#38507, $t = 4.351$ s)*
The percentage error on the intensity obtained from the LUT as a function of the LOS is shown in figure 5(a). The relative error is in the range of 1%, showing a good agreement between the two calculations. The half and one third energy components are subject to an additional approximation. The LUT is built using the neutrals at full energy, while the other two components are obtained by dividing the injection energy by a factor two and three, respectively. This results in worse agreement with respect to the full energy component and the halo neutrals. These last two neutral components show a percentage error well below 1% for each LOS. The results show that the parameter grid chosen for the LUT is appropriate and, from now on, only different shots from the reference one will be analysed.

(ii) *Shot from the same experimental campaign (#39648, $t = 5.375$ s)*
#39648, from the same experimental campaign as the reference shot, features a higher density ($n_e = 7.26\times10^{19}$ m$^{-3}$). As expected, the errors shown in figure 5(b) have now increased, but remain well below 10% for each LOS. This result shows that the LUT could also be applied in the analysis of a different shot from the same experimental campaign as the reference one.

(iii) *Shot from a different experimental campaign (#30809, $t = 4.48$ s)*
As a last test, the relative error on the FIDA intensity is calculated for a discharge from a different experimental campaign. This shot features a lower density ($n_e = 3.9\times10^{19}$ m$^{-3}$) and, in addition to NBI heating, also ICRH is used. Between different campaigns, the lines of sight can be displaced by some millimetres and this change of geometry introduces an additional distinction between the analysed shot and the reference one. In this case, the CER lines are displaced between 3 mm and

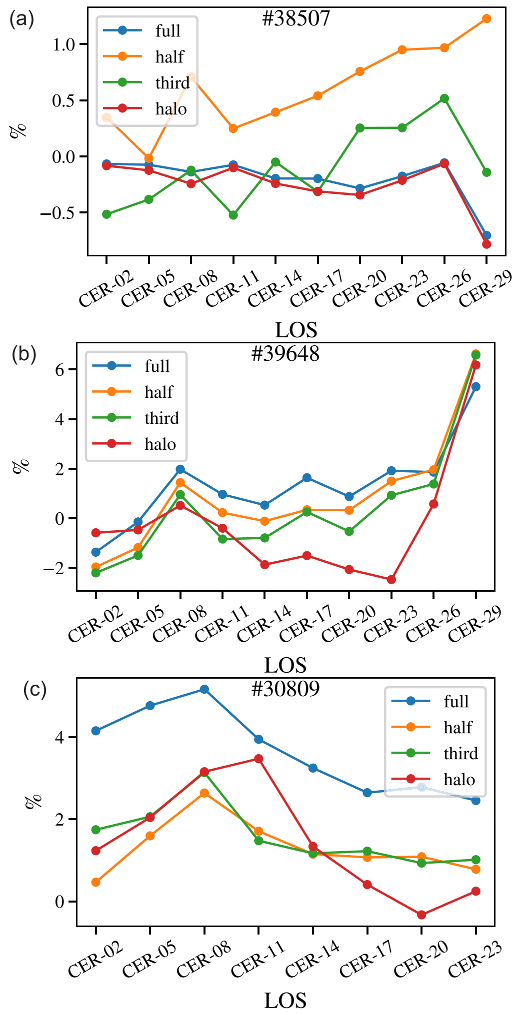


**Figure 5.** Percentage error on the FIDA emission obtained from the look-up table, relative to each neutral component and toroidal line of sight of ASDEX Upgrade for: (a) #38507, (b) #39648 and (c) #30809. CER-02 is the innermost LOS ($R = 1.7$ m), increasing the number associated to the CER line, the radial position moves towards the edge, ending with CER-29 ($R = 2.1$ m). The relative error increases starting from the reference shot, moving to a different shot form the same experimental campaign and ending with a discharge from a different one. Nevertheless, the error always stays well below 10%.

4 mm with respect to #38507. The results obtained are shown in figure 5(c). Making a comparison with figure 5(b), the range of percentage errors has not increased. However, while previously only a few LOS were above 3%, the values are now on average larger. In conclusion, these results suggest that the impact of the different lines of sight's geometry might remain within an acceptable range of agreement.

## 5. Analytic weight functions

Once obtained the $\lambda$-independent $R$ functions from the LUT, we need to calculate the probability of the emission in a determined wavelength range (equation (3)). The probability $\mathrm{prob}(\lambda_1 < \lambda < \lambda_2 | E, p, \phi)$ depends on the Doppler shift, on the Stark splitting and on the collisional radiative processes, which are all related to the ion gyro-angle at the moment of the CX reaction.

The analytic expression for the emission probability has been derived in [11] and is given by:

$$\mathrm{prob}(\lambda_1 < \lambda < \lambda_2 | E, p, \phi) = \sum_{l=1}^{15} \left( \int_{\gamma_{2,l}}^{\gamma_{1,l}} \mathrm{prob}(l|\gamma) pdf_{D_\alpha}(\gamma|E,p) d\gamma + \int_{\gamma'_{1,l}}^{\gamma'_{2,l}} \mathrm{prob}(l|\gamma) pdf_{D_\alpha}(\gamma|E,p) d\gamma \right) \tag{5}$$

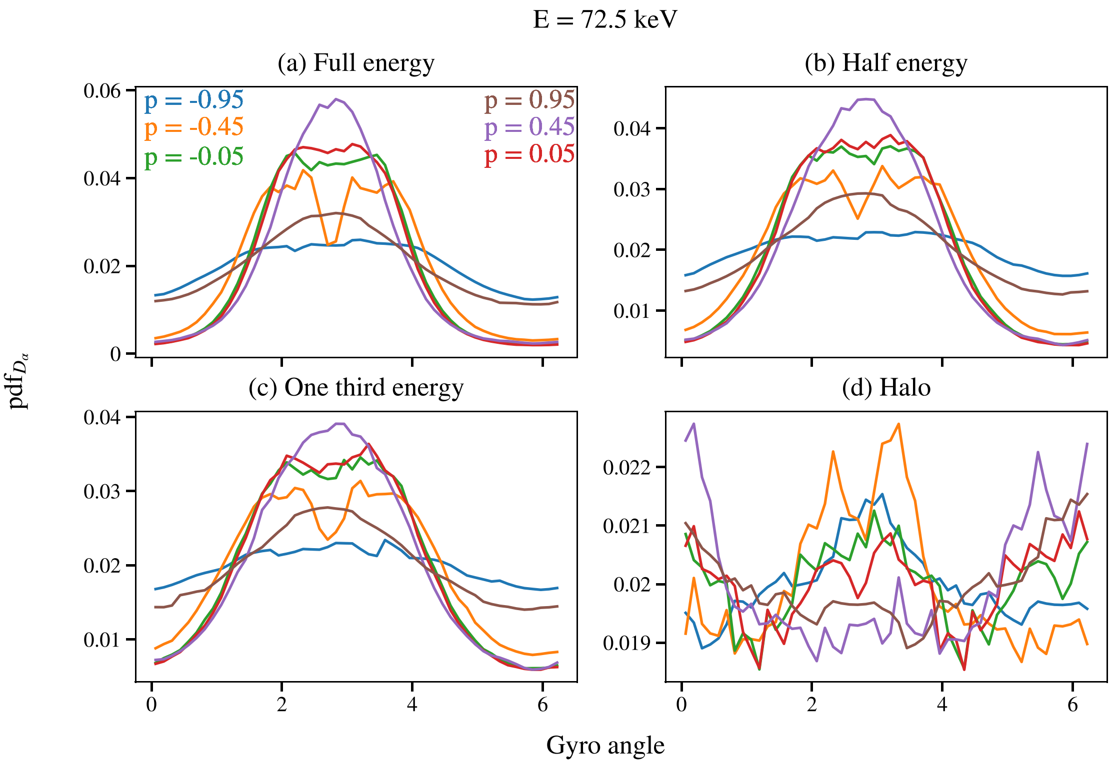


**Figure 6.** $pdf(\gamma|E,p)$ relative to #38507 at $R = 1.71$ m. The energy is 72.5 keV and the pitch is fixed at six different values. For the beam neutrals, the probability distribution function associated to $p = \pm 1$, i.e. the fast ion is moving parallel to the magnetic field, is close to a uniform distribution ($pdf_{D_\alpha} = 1/2\pi$). Increasing the pitch, the amplitude of $pdf_{D_\alpha}$ increases, denoting a stronger dependency of the $D_\alpha$ emission on the gyro-angle. Differently from the beam neutrals, the thermal halo slightly deviate from a uniform distribution for every pitch. In addition, increasing the energy, the amplitude increases and vice versa. It is stressed how modelling $pdf_{D_\alpha}$ as a cosine function would represent a rough approximation, leading to big deviations from the expected intensity.

where $l$ stands for the Stark line and $\gamma$ is the gyro-angle. The limits of integration $\gamma_1$ and $\gamma_2$ correspond to the boundaries of the wavelength interval $\lambda_1$ and $\lambda_2$, respectively. $\mathrm{prob}(l|\gamma)$ is the probability that a detected photon, given the gyro-angle, comes from the line $l$ of the Stark splitting, which can be analytically computed. $pdf(\gamma|E,p)$ is the probability density function of the $D_\alpha$ emission as a function of $\gamma$. The emission is not equally probable for all gyro-angles, since the latter are related to the charge-exchange and electron transition probabilities. These probabilities are determined by the cross-sections $\sigma(\mathrm{v_{rel}})$ and the relative velocity $\mathrm{v_{rel}}$. The relative velocity, in turn, depends on energy, pitch and gyro-angle of the fast ion, as well as on the neutral species involved in the reaction, i.e. beam neutrals or thermal halo. These neutral populations themselves depend on the specific NBI source. A simple cosine model for $pdf(\gamma|E,p)$, as proposed in [11], was tested but found to be unsatisfactory. For this reason, and to avoid introducing additional approximations, the probability density function is computed numerically using FIDASIM. An example $pdf(\gamma|E,p)$ of the $D_\alpha$ emission for each neutral component of #38507, at a fixed energy and at six different pitch values, is shown in figure 6: (a) full energy component, (b) half energy component, (c) one third energy component and (d) halo neutrals.

We now have all the ingredients to calculate the probability of the emission in a determined $\lambda$ range, according to equation (5). Once this is known, the weight function can be reconstructed using equation (3). To make a qualitative comparison, a weight function computed both with FIDASIM and with the analytical formula is shown in figure 7.

To quantify the introduced approximations, the percentage error in the FIDA emission intensity computed using analytical weight functions is evaluated against FIDASIM results. The results obtained for each neutral component of #38507 are shown in figure 8. The relative error on each neutral component stays within 10%. In addition, since the experimentally measured FIDA emission corresponds to the total signal, the contributions from each neutral component are summed together. By doing this, the relative error reduces to 3%. Note that the relative error in the total FIDA emission is not equal to the sum of the individual component errors, since each component contributes differently to the total, with the halo and the full energy component dominating. The result obtained indicates that the analytical formula is precise enough to reproduce the FIDA intensity for our purposes.

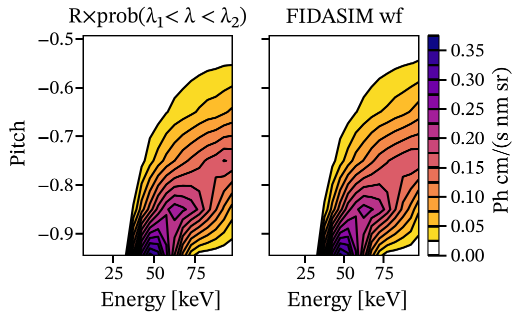


**Figure 7.** Qualitative comparison between a weight function (#38507, $t = 4.351$ s, $R = 1.71$ m) obtained from the analytic calculation and from FIDASIM. Since in FIDASIM's calculation the factor $1/(4\pi\,\mathrm{d}\lambda)$ is included inside the weight function, $R(E,p)prob(\lambda_1 < \lambda < \lambda_2|E,p,\phi)$ must be multiplied by the same factor to obtain [Ph cm/(s nm sr)]. The plot is zoomed in the region where the weight function is different from zero. A very good agreement between the two calculations is observed.

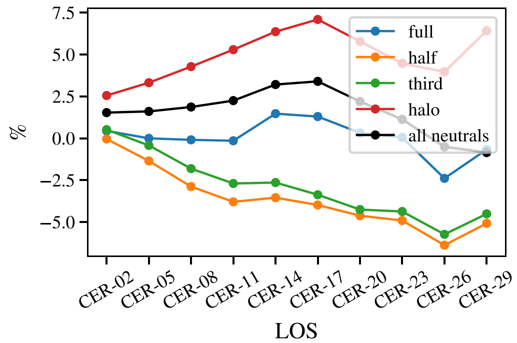


**Figure 8.** Comparison between the FIDA emission intensity computed by FIDASIM and with the analytic formula for each toroidal LOS and neutral component. In addition, the total emission is obtained as the sum of the intensities due to all the neutrals. The percentage error associated to the latter, shown in black, is kept within 3%. The results always refer to #38507 at $t = 4.351$ s and $\lambda$ in [660, 661] nm.

### 5.1. Combination of analytic weight functions and $\tilde{R}$ LUT

Once the performance of the analytical formula has been tested, it can be used to get the FIDA intensity from the LUT built for the $\tilde{R}$ functions. This step combines the approximations of the LUT, estimated to be within 10% in section 4, to the ones due to the analytical formula. Concerning the latter, further inaccuracies are introduced when employed in the analysis of an arbitrary shot. Indeed, $pdf(\gamma|E,p)$ needs to be numerically computed with FIDASIM, which is not compatible with a fast evaluation of the FIDA diagnostic. For the purpose of this work, it has been decided to store the probability density function of the $D_\alpha$ emission for the reference shot in a file and to use it in the analysis of each discharge. This is again a strong assumption, since $pdf(\gamma|E,p)$ depends on the reaction probabilities and, in turn, on the neutral distribution, which changes between different discharges. We underline that the stored $pdf(\gamma|E,p)$ refers to the NBI source Q3, on which the FIDA diagnostic is aligned. Despite this drawback, we have the advantage that the calculation of $\mathrm{prob}(l|\gamma)$ is made using the actual magnetic field $\mathbf{B}$ and projection angle $\phi$ of the analysed shot. The latter allows us to introduce the effects of the real geometry of the lines of sight of the specific discharge, since up to this point only that of the reference shot has been used.

The intensities computed with FIDASIM and with the LUT for the same discharges studied in section 4, belonging to both the same and a different experimental campaign with respect to the reference shot, are compared to each other. Before showing the results, the procedure to get the weight function from the LUT is briefly summarized. Using as target the previously computed line averaged plasma parameters, the four dimensional interpolation on the parameters grid is performed. The obtained $\tilde{R}$ function is then multiplied by the actual line integrated neutral density of the analysed discharge. Last, the $R$ function thus calculated is multiplied by the analytical emission probability to reproduce the weight function.

The outcome of the comparison is summarized in the following:

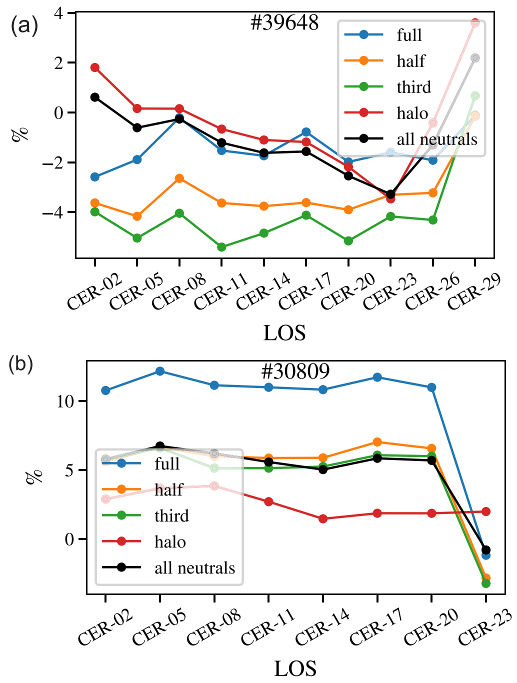


**Figure 9.** Percentage error on the FIDA emission obtained with the look-up table coupled with the analytical formula for: (a) #39648 and (b) #30809 in the $\lambda$-range [660, 661] nm. The neutral components are shown separately and, then, they are summed together to find the total FIDA emission (shown in black). Compared to figure 5, the approximations introduced with the analytical formula translate in an increased relative error. Anyway, the one on the total emission, estimated within 6%, is still performing in an acceptable range.

(i) *Shot from the same experimental campaign (#39648)*
The percentage error on each neutral component and on the total FIDA emission for each toroidal LOS of the FIDA diagnostic is shown in figure 9(a). Concerning the separate neutral components, the error stays within 5%. Comparing the plot with figure 5(b), where the same comparison is performed without the additional approximations introduced by the analytical formula, it is possible to assess how the error has increased for each LOS. Nevertheless, the relative error on the total FIDA emission stays within 3% (see black line in figure 9(a)). The latter result shows that, given all the approximations introduced up to this point, the new method allows to reproduce the total FIDA emission within the target uncertainty range.

(ii) *Shot from a different experimental campaign (#30809)*
Figure 9(b) shows that, for this discharge, the percentage error stays within 11% for all the neutral components and toroidal lines of sight. As done before, since the FIDA diagnostic is looking at the total emission, the intensities due to all the neutral components are summed together. The relative error on the total FIDA emission now stays within 6%. Making a comparison with #39648, a worsening in the percentage errors can be clearly observed. This could indicate that, when using the analytical formula with $pdf(\gamma|E,p)$ of the reference shot, the change in the lines of sight's position plays a role.

It can now be discussed if the approximations introduced by the analytic calculation can be accepted or if it is better to build the LUT for the weight functions. The latter would reduce the approximations, but it would increase in dimension according to the number of wavelength ranges included and would lack flexibility. In particular, the number of wavelength ranges and their width would be fixed. By contrast, using the analytical formula, the $\lambda$-range can be chosen as desired. Indeed, a LUT made for the $\tilde{R}$ functions is advisable. However, the impact of the approximations introduced within the analytical calculation must be evaluated in the context of all the other steps of the fast method and the desired level of confidence in the final result. This point will be discussed again when presenting the results obtained with the fully developed new fast method.

# 6. Fast neutral model

The calculation of the $\tilde{R}$ function via the LUT requires prior knowledge of the line integrated neutral densities and line averaged plasma parameters of the discharge considered. For a fast analysis, a fast neutral model able to reproduce the neutral population and to calculate the above mentioned LOS-related quantities is needed.

We decided to implement the neutral calculation inside the RABBIT code [13]. The latter is able to simulate the NBI fast-ion distribution in real-time. To this end, it is equipped with a simplified model for the beam geometry and attenuation, i.e. the population of beam neutrals was already available within the code. However, a model for the halo neutrals was missing. In addition, routines to include the LOS geometry were also not present.

First, we incorporate the geometry of the lines of sight into the code, enabling the calculation of the line integrated neutral densities and line averaged plasma parameters. The profiles of the plasma parameters are given to the code as input. Last, a fast model for the halo neutrals is implemented to obtain the same LOS-related quantities for this neutral component as well. Each one of these steps is described and discussed in detail in the following.

## 6.1. LOS geometry

The calculation of the line integrated neutral densities and of the line averaged plasma parameters needs, in the first instance, the information about the LOS geometry.

Within RABBIT, the beam attenuation, based on BESFM [16], is modelled in one dimension along the beam centreline, using a coordinate $l$ aligned with it. The latter is divided in a fixed number of points distanced by default by $\mathrm{d}l = 0.01$ m, which can be changed flexibly. The shape of the beam is described by a Gaussian in the plane perpendicular to $l$, whose width $\sigma$ diverges penetrating inside the plasma, according to $\sigma(l) = a_1 + a_2 l + a_3 l^2$. The lines of sight of the FIDA diagnostic are closely looking at the beam axis, which represents the source of the neutral particles. The geometry of the LOS is prepared according to the beam coordinate system, in order to facilitate the calculation.

Each LOS is divided in a fixed number of points, in each of which we have to calculate the neutral density. To get the density at a given point, the point is projected onto the beam axis and the 1D neutral density is evaluated at the corresponding projected coordinate $l_\mathrm{P}$. This value is then multiplied by a beam profile function and by a factor converting the density from 1D to 3D:

$$n_{3\mathrm{D}}\left(P_{\mathrm{LOS}}\right) = n_{1\mathrm{D}}\left(l_\mathrm{P}\right) \exp\left(-\frac{\mathrm{d}^2_{\mathrm{P_{LOS}}-l_\mathrm{P}}}{2\sigma\left(l_\mathrm{P}\right)^2}\right) C_{3\mathrm{D}} \tag{6}$$

where $n_{1\mathrm{D}}(l_\mathrm{P})$ is the density along the beam, $d_{P_{\mathrm{LOS}}-l_\mathrm{P}}$ is the distance between the point on the LOS and the projected point, $\sigma(l_\mathrm{P})$ is the width of the beam in the projected point and $C_{3\mathrm{D}}$ is the constant to pass from one to three dimensions. The latter can be found putting equation (6) inside

$$n_{1\mathrm{D}} = \int\int n_{3\mathrm{D}}\,\mathrm{d}A. \tag{7}$$

The resulting constant is $C_{3\mathrm{D}} = \frac{1}{2\pi\,\sigma(l_\mathrm{P})^2}$.

In this way we get the neutral density along each LOS, which will be needed for further calculations.

## 6.2. Beam Neutrals

The simulation of the beam neutrals within RABBIT, based on [16], consists of the solution of the collisional radiative model along the beam. The model accounts for ionization, impact excitation and de-excitation with electrons, ions and impurities, charge-exchange reactions with ions and impurities and spontaneous de-excitation. Before entering the plasma, all the neutrals are assumed to be in ground state. In the time evolution, the number of atomic states considered is usually set to $n \leqslant 2$ to reduce the computational time. The collisional radiative model returns the evolution of the beam density along $l$, i.e. the density in [1/m] in each point sampled along the beam axis. The model takes into account the three beam neutral components separately.

For our model we calculate the following LOS-related quantities:

(i) *Line integrated neutral density*
The line integration is performed summing the neutral density, multiplied by $\mathrm{d}l_{\mathrm{LOS}}$, in each point along the LOS:

$$n_{\mathrm{int,j}} = \int_{\mathrm{LOS}} n_{\mathrm{3D,j}}\left(P_{\mathrm{LOS}}\right)\, \mathrm{d}l_{\mathrm{LOS}} \tag{8}$$

with $j = E$, $E/2$ or $E/3$, i.e. each beam component is treated separately.

(ii) *Line averaged plasma parameters*

The plasma parameters required from the LUT for the beam neutrals are $n_\mathrm{e}$, $Z_{\mathrm{eff}}$ and $T_\mathrm{e}$. As already introduced in section 2, the line averaged plasma parameters are weighted over the neutral beam density:

$$k_{\mathrm{mean}} = \frac{\sum_{i=1}^{n_{\mathrm{pts}}} k_\mathrm{i}\, n_{\mathrm{i,j}}\, \mathrm{d}l_{\mathrm{LOS}}}{\sum_{i=1}^{n_{\mathrm{pts}}} n_{\mathrm{i,j}}\, \mathrm{d}l_{\mathrm{LOS}}} \tag{9}$$

with $k$ plasma parameter and $j = E$, $E/2$ or $E/3$.

### 6.3. Halo Neutrals

The simulation of the halo neutrals was not previously included within RABBIT and therefore we implemented it from the ground up. The first step consists of finding an appropriate model to describe the halo population that is consistent with RABBIT's beam model and meets the requirement of a fast computation.

At first, a simplified halo model taken from the FAST code and employed within CHICA (equation (10) in [17]) was tested. The approximations introduced by this model were leading to relative errors in the final results exceeding 20%. For this reason, given the importance of the halo neutrals in determining the emission intensity, we decided to reproduce the halo population making use of a LUT. The latter is built with FIDASIM using the reference shot #38507, and stores the ratio between the halo density and the beam density gradient along the beam axis and the width of the halo cloud in the two directions perpendicular to the beam centreline. The choice of storing the halo density over the beam density gradient comes from the physical processes that generate the halo neutrals. The first generation of halo neutrals, produced by direct charge exchange (DCX), is created by the CX reaction between beam neutrals and thermal ions. The DCX neutrals can be lost due to ionization or further charge exchange with thermal ions. In the case of ionization, the neutral particle is lost, whereas in the case of CX the loss of the DCX neutral is balanced by the creation of a new neutral particle. This process establishes a chain reaction in which the newly created neutrals can undergo further CX with thermal ions, leading to several generations of halo neutrals. In summary, the primary source of the halo neutrals is the neutral beam. In particular, the number of halo neutrals generated is proportional to the number of beam neutrals lost through charge exchange, i.e. to the beam density gradient. In addition, to be able to obtain an evaluation of the spatial extent of the halo population, the LUT stores the width of the cloud. The latter is just an approximation, obtained as the standard deviation of the halo density in the two directions perpendicular to the beam axis in FIDASIM's beam grid. Each quantity stored in the LUT is evaluated for each point on a plasma parameter grid and for each position along the beam.

When using the LUT to obtain the halo density within RABBIT, differences with respect to FIDASIM in the beam simulation and attenuation need to be considered. FIDASIM employs a full 3D Monte Carlo simulation and thus provides a good benchmark for our fast method, whereas RABBIT computes the neutral population only up to the separatrix. Consequently, the beam density gradient leads to a zero halo density outside the plasma and to a steep increase at the separatrix. In FIDASIM, instead, the halo density increases gradually since also retrodiffusion is considered, i.e. the halo neutrals generated at a given position along the beam axis can contribute to the population present both toward the core and toward the edge. To reproduce this phenomenon into RABBIT, the beam density gradient is averaged over a gaussian as follows:

$$\nabla n_{\mathrm{avg}}\left(l_0\right) = \frac{\int \nabla n\left(l\right)\, \exp\left(-\frac{l-l_0}{2\sigma^2}\right)\, \mathrm{d}l}{\int \exp\left(-\frac{l-l_0}{2\sigma^2}\right)\, \mathrm{d}l} \tag{10}$$

$\nabla n_{\mathrm{avg}}$ at position $l_0$ contains the contribution of the beam density gradient in each point along the beam, with the corresponding weight, determined by an arbitrary $\sigma$. This is done to mimic the complex motion of neutral particles in FIDASIM, which takes into account their behaviour immediately before and after the considered position. If $\sigma$ is set to values smaller than the sampling distance $\mathrm{d}l$ between the points along the beam in RABBIT, $\nabla n_{\mathrm{avg}}$ is equal to $\nabla n$. As $\sigma$ increases, the profile gradually becomes flatter. For this reason, with $\mathrm{d}l = 1$ cm, we found that a suitable choice is $\sigma = 2$ cm. As an example, figure 10 shows the superposition of the halo population computed by the two codes for #30809. Besides

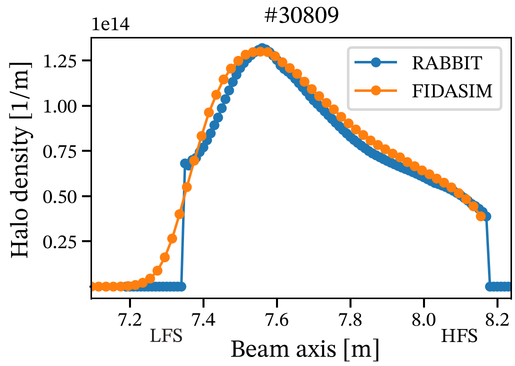


**Figure 10.** Superposition of the one-dimensional halo density along the beam axis obtained from FIDASIM and RABBIT. In the region where the beam enters the plasma, the difference between the two codes is immediately visible. RABBIT computes the neutral density only in the confined plasma region. After reaching the halo density peak, other smaller discrepancies are introduced by the different beam attenuation calculation performed in the two codes.

**Table 2.** Table summarizing the approximations introduced in the fast method, along with the step at which each is applied, compared to FIDASIM weight function calculation.

| Step | Approximations |
|---|---|
| Fast-ion distribution function | TRANSP: same as FIDASIM RABBIT: approximate real-time simulation |
| Fast model for neutral densities (RABBIT) | Different beam attenuation LUT for halo neutrals |
| Weight function calculation | LUT for $\tilde{R}$ analytical formula for $prob(\lambda_1 < \lambda < \lambda_2 \vert E, p, \phi)$ tabulated $pdf_{D_\alpha}(\gamma \vert E, p)$ |

small discrepancies, the approximated method employed within RABBIT is able to reproduce both the trend and the values assumed by the halo density along the beam axis.

Once the halo density along the beam is obtained, the line integration can be performed and the line averaged plasma parameters can be calculated.

(i) *3D neutral density and line integration*
Before performing the line integration, the linear density must be converted into a 3D density. The conversion is similar to equation (6), but extended to account for the two independent widths of the halo cloud, obtained from the LUT, along the axes perpendicular to the beam centreline. The line integrated halo density is again obtained with equation (8).

(ii) *Line averaged plasma parameters*
The line averaged plasma parameters are obtained with the same procedure explained for the beam neutrals, by applying equation (9). The only difference is that the LUT for the halo neutrals, in addition to $n_\mathrm{e}$, $Z_\mathrm{eff}$ and $T_\mathrm{e}$, requires the calculation of the line averaged $T_\mathrm{i}$.

## 7. Verification of the fast method

Now we have discussed all the components of the new fast method, as outlined in the flowchart in figure 4, and we can test it against FIDASIM. The approximations introduced, together with the corresponding steps, are listed in table 2. The verification is made employing the fast-ion distribution simulated with TRANSP and used in FIDASIM. In this way it is possible to identify the relative error arising just from the approximations introduced by the new method.

In figure 11, the relative error on the FIDA emission intensity obtained with the new method for each toroidal LOS of the same discharges analysed in the previous sections, #39648 and #30809, is shown.

Despite all the approximations introduced in the different steps of the new method, the percentage error on the total FIDA emission (shown in black) remains within 10%. Considering the large uncertainty in the experimental FIDA intensity calibration, the result obtained can be considered acceptable and the new method is deemed to perform reliably.

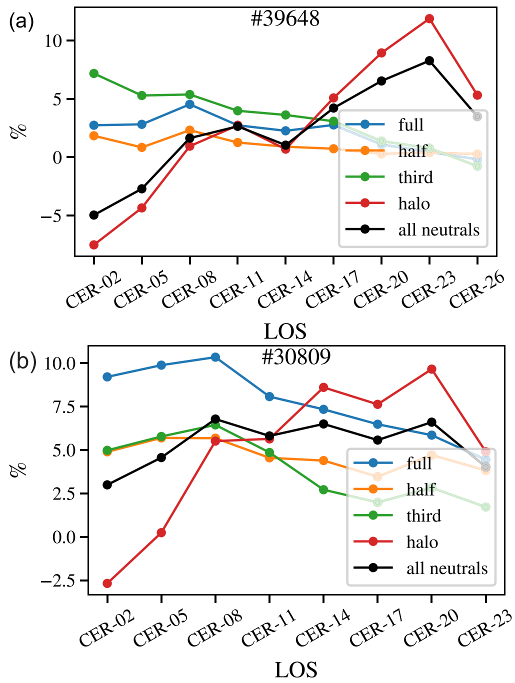


**Figure 11.** Relative error on the FIDA emission obtained with the new method as a function of the toroidal lines of sight for: (a) #39648 and (b) #30809 in the $\lambda$-range [660, 661] nm. We recall that CER-02 is the innermost line, while CER-26 is the outermost one. Again, the black line refers to the error on the total emission, which is the one we need to compare the simulated spectrum with the experimental one.

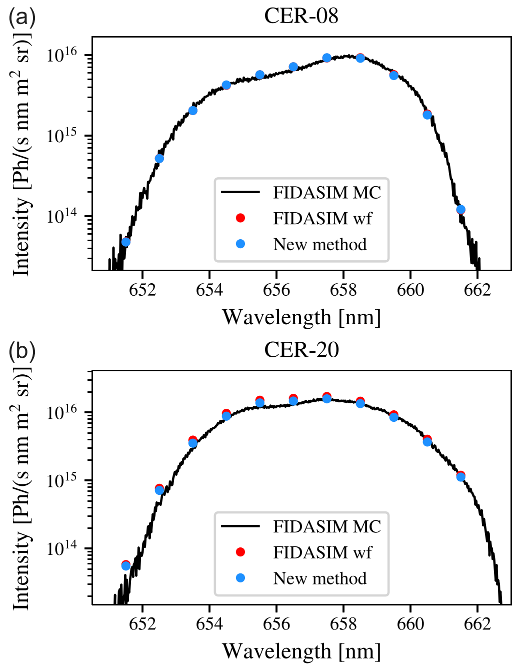


**Figure 12.** A whole spectrum obtained with the standard FIDASIM Monte Carlo simulation is shown in black in logarithmic scale. Superposed to it, the intensity in a set of different wavelength ranges calculated both with FIDASIM weight function approach, in red, and with the new method, in blue, is displayed. The discharge is #39648 and the lines of sight are: (a) CER-08, located at $R = 1.79$ m and (b) CER-20, located at $R = 1.97$ m.

All the comparisons presented so far refer to the fixed wavelength range [660, 661] nm. However, the new fast method allows the selection of an arbitrary wavelength range and the reconstruction of a whole spectrum. Fixing a LOS, the emission intensity is now calculated for a set of wavelength ranges both with FIDASIM and with the new method. The results obtained choosing an inner and an outer CER LOS, superposed to a whole Monte Carlo spectrum, are shown in figure 12: (a) CER-08 and (b) CER-20. The nice match obtained between the calculations can be clearly observed. However, the region we are interested in is the one starting around 660 nm, i.e. some nanometres shifted from the other components of the $D_\alpha$ spectrum, where we can isolate the emission only due to the fast-ions.

At this point we can comment further on the last remark of section 5. Overall, with the new method we are able to keep the relative error on the total FIDA emission within 10%, our defined target, and well below this threshold for most CER lines of sight in both discharges #39648 and #30809. Based on these results, creating a LUT for the $\tilde{R}$ functions proves to be a more effective approach than doing so for the weight functions, due to the flexibility in the choice of the analysed wavelength range. This conclusion may, however, be reconsidered if higher accuracy is required.

In such cases, it would also be possible to create a LUT specific to each experimental campaign, thereby recovering the correct LOS geometry. Nevertheless, the preferred approach is to use a single LUT consistently. The results indicate that the error introduced by millimetric displacement of the lines of sight remains within the target uncertainty range, supporting the reuse of the LUT as valid approximation.

## 8. Summary and outlook

In this work, we have developed a fast method to reproduce the FIDA emission intensity, based on the FIDASIM weight function approach. The new method enables a significant reduction in computational time by avoiding FIDASIM calculation, reproducing the weight functions through a LUT for the $\tilde{R}$ functions and an analytical formula for prob($\lambda_1 < \lambda < \lambda_2$|E, p, $\phi$). This reduces the simulation time per time point from minutes to near real-time performance, with the fast-ion distribution function simulation excluded from this estimate. The LUT requires the knowledge of the line integrated neutral densities and of the line averaged plasma parameters, which are obtained through a fast neutral model implemented for this purpose within the RABBIT code.

The work is focused on reproducing the FIDA emission intensity along the toroidal lines of sight of AUG, which are the ones with the best radial resolution. The relative error on the results obtained with the new fast method compared to FIDASIM is kept within 10% for each CER LOS of the analysed discharges. We can state that the new method performs as intended, although discrepancies may arise when the experimental conditions differ from those of the reference shot. The LUT is not a flexible tool and, for example, we are storing the $\tilde{R}$ functions from a shot in which only NBI Q3 is active. If other beams of box 1 are active, the neutral distribution is subject to changes. The reference discharge features a common set-up for FIDA measurements, but possible differences need to be taken into account.

The main goal of a fast analysis of FIDA data is the possibility to reproduce the emission over whole discharges, in order to study the evolution of the fast-ion distribution. By comparing the forward-modelled FIDA signal with experimental data, discrepancies can be identified and used to infer fast-ion transport. The reduced computational times enable the systematic study over large numbers of discharges, allowing the identification of trends and of relevant time points, thereby improving our understanding of fast ion behaviour.

The prerequisite of this approach is the availability of a fast-ion distribution function. TRANSP simulations over hundreds of time points can be used to reproduce the trend of the FIDA emission over entire discharges. However, due to TRANSP long computational times, this approach is not compatible with a fast analysis. To speed up the whole calculation, we need to integrate within the new method the real-time simulated fast-ion distribution function provided by RABBIT. While FIDA measurements are typically localized on the low field side, RABBIT calculates the flux surface averaged distribution function, introducing inaccuracies. How to interface the RABBIT distribution function with the new method and how to mitigate the resulting uncertainties is currently under investigation. This final step will enable the study of entire discharges on real-time timescales and may pave the way for real-time FIDA applications.

## Data availability statement

No new data were created or analysed in this study.

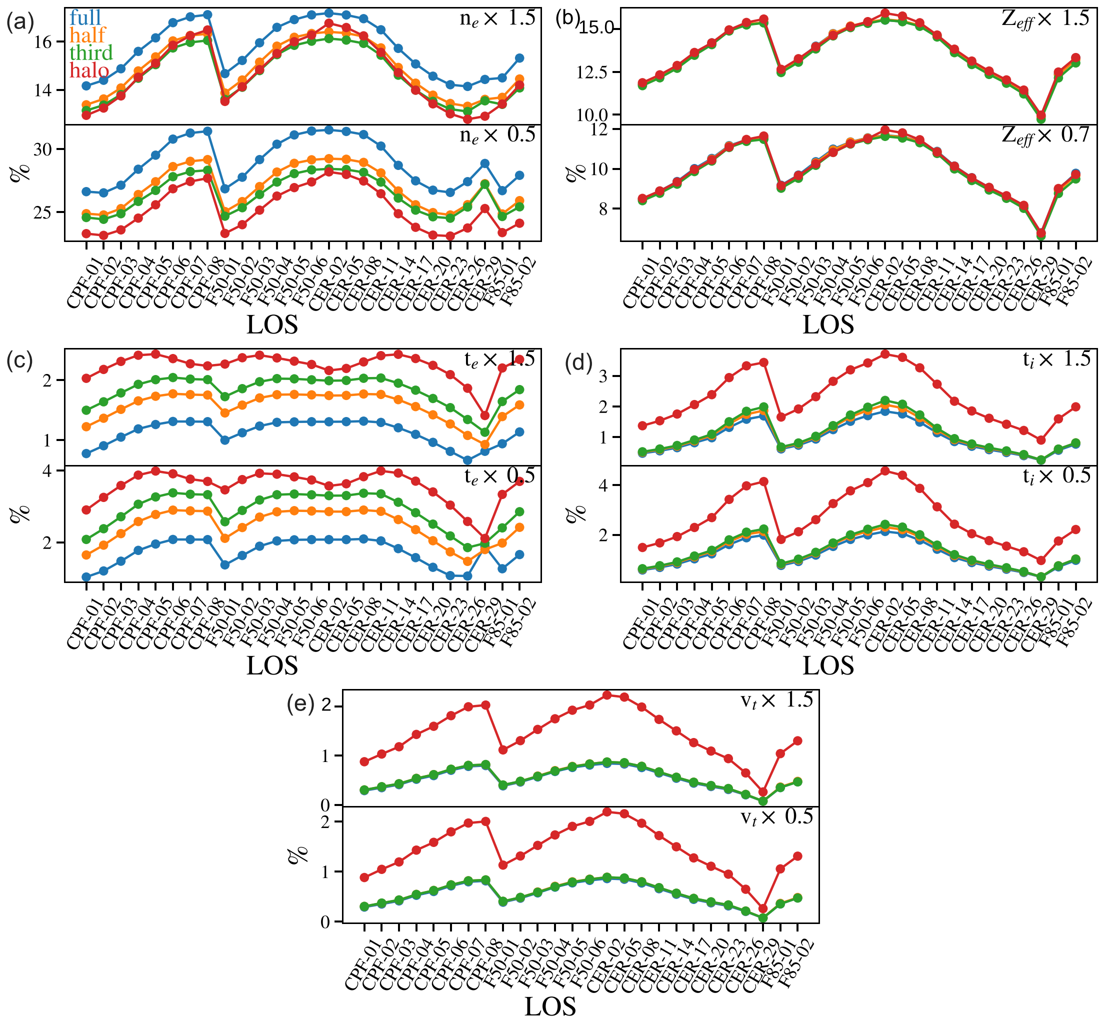


**Figure 13.** Sensitivity study performed on: (a) $n_e$, (b) $Z_{eff}$, (c) $T_e$, (d) $T_i$ and (e) $v_t$. The parameters showing stronger variations are $n_e$ and $Z_{eff}$. Weak variations are observed for $T_e$ and $T_i$. $v_t$ can be considered negligible for all the neutral components.

## Appendix A. Sensitivity study

The plots showing the sensitivity study performed on each plasma parameter are shown in figure 13: (a) $n_e$, (b) $Z_{eff}$, (c) $T_e$, (d) $T_i$ and (e) $v_t$. Each profile is increased and decreased, keeping all the other parameters fixed. The ranges covered by the profiles are (approximately): $n_e$ in [4–7] $\times 10^{19}$ 1 m$^{-3}$, $T_e$ in [1–4] keV, $T_i$ in [1–6] keV and angular frequency in [1.1–0.2] $\times 10^5$ rad s$^{-1}$. The effective charge has the nominal value of 1.82. The $R$ function obtained with the modified parameter is compared to the reference one for each line of sight (LOS), following the metric:

$$\left(\sum_{E,p} \frac{\left(R_{\text{reference}}(E,p) - R_{\text{modified}}(E,p)\right)^2}{R^2_{\text{reference}}(E,p)} \times \frac{1}{n_E \cdot n_p}\right)^{\frac{1}{2}}$$

with $n_E$ and $n_p$ number of energy and pitches, their product is the actual length of $R$. The metric is expressed as percentage in the plots and denoted as %.

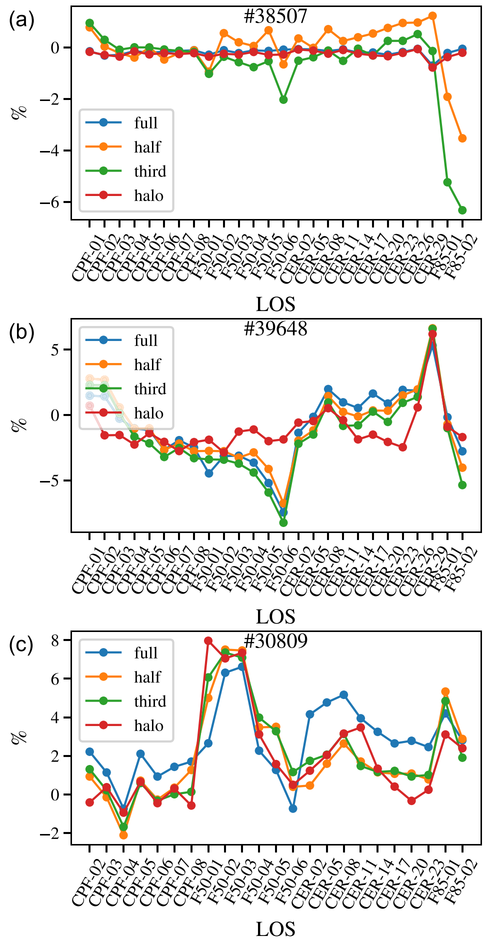


**Figure 14.** Percentage error on the FIDA emission obtained from the look-up table, relative to each neutral component and line of sight of ASDEX Upgrade for: (a) #38507, (b) #39648 and (c) #30809. The CPR lines are poloidal LOS, CPF-01 is the outermost, while CPF-08 is the innermost. Both F-50 and F-85 are radial LOS, with identification numbers starting from the edge and increasing approaching the core. Last, we find again the toroidal lines, with CER-02 the innermost one. For all the three analysed discharges, the error always stays below 10%.

## Appendix B. Verification of the fast method for the full set of Fast-Ion $D_\alpha$ (FIDA) lines of sight

Each step of the new fast method has been tested for all the lines of sight of the FIDA diagnostic of ASDEX Upgrade. In addition to the toroidal (CER) LOS, the diagnostic is equipped with poloidal (CPF) and radial (F-50 and F-85) lines of sight, which are identified with increasing numbers toward the core. A detailed description of the lines of sight geometry is provided in [4].

The ability of the look-up table (LUT) to reproduce the FIDA intensity (section 4.3) for all the lines of sight is shown in figure 14: (a) #38507, (b) #39648 and (c) #30809. The percentage error is kept below 10%, as desired.

The second step consists of reproducing the FIDA emission intensity using the LUT for the $\tilde{R}$ functions and the analytical formula for the $D_\alpha$ emission probability (section 5.1). The relative error associated to each LOS is reported in figure 15: (a) #39648 and (b) #30809. The total FIDA emission is always kept within 10%, except for CPF-08 in discharge #30809.

Finally, adding the line integrated neutral densities and line averaged plasma parameters calculated by RABBIT (section 7), the relative error on the full fast method is calculated for each LOS and shown in figure 16.

The crossing of the 10% threshold in the poloidal lines of sight is clearly visible. The observed discrepancy between the new method and FIDASIM is attributed to the calculation of the line integrated halo density. The overestimation of this quantity within RABBIT, compared to FIDASIM, is observed for both shots and increases from the core CPF LOS toward the edge. This results in an overestimation of the intensity. The main difference between the various lines of sight lies in their geometry: the CPF lines look into the halo cloud in the poloidal direction, while the CER in the toroidal one. Given the

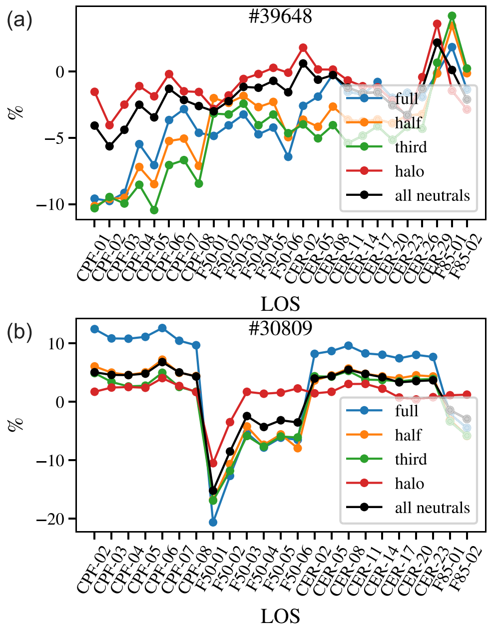


**Figure 15.** Percentage error on the FIDA emission obtained with the look-up table for the $\tilde{R}$ functions coupled with the analytical formula for: (a) #39648 and (b) #30809. The total FIDA emission, shown in black, is kept within 10% as desired. The only exception is CPF-08 in discharge #30809.

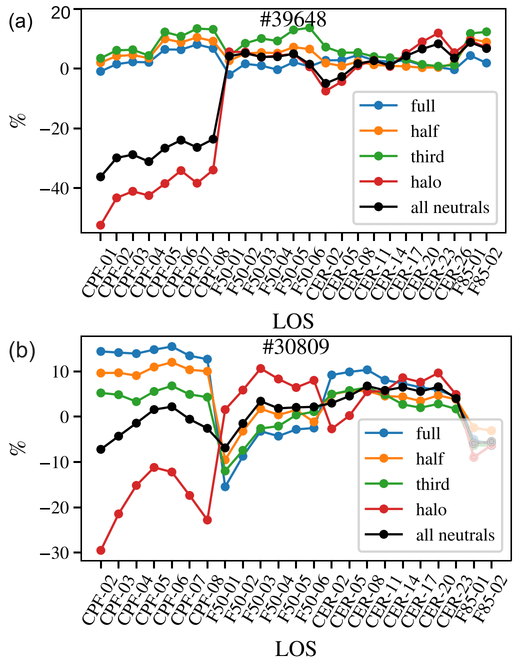


**Figure 16.** Percentage error on the FIDA emission obtained with the whole new fast method for: (a) #39648 and (b) #30809. An increased relative error on the CPF lines of sight, due to the line integrated halo density calculation in the poloidal direction, is observed. Only for those LOSs, the total FIDA emission, shown in black, is not kept within 10%.

difficulty of reproducing the shape of the halo cloud (section 6.3), the observed discrepancies may arise from the approximations used in the calculation of the cloud width. For #39648 the total FIDA emission stays within 10% for all the LOS, apart from the CPF (i.e. the ones showing the biggest relative error on the density estimation). For #30809, the total FIDA emission is always estimated within the target error range, but it must be highlighted that this is due to the compensation between the overestimation of the beam emission and the underestimation of the halo one.

We recall that all the relative errors are calculated with respect to a single FIDASIM simulation, however, since the neutrals are obtained via a Monte Carlo method, each run yields slightly different results.

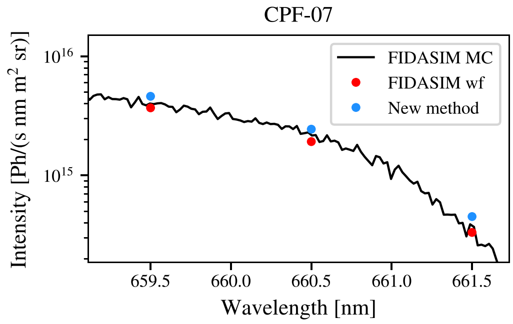


**Figure 17.** Superposition of the Monte Carlo spectrum and of the intensities obtained with FIDASIM weight function calculation and with the new fast method in the wavelength ranges [659, 660] nm, [660, 661] nm and [661, 662] nm. The discharge is #39648 and the LOS is CPF-07 ($R = 1.76$ m), where the relative error between FIDASIM weight function method and the new fast method is higher than 20%. The plot aims at highlighting why we searched for a small relative error in the CER lines, where a nice match between the Monte Carlo and the weight function simulations is observed.

When comparing the results obtained with the new method to different FIDASIM runs, the relative error can vary by up to 4%.

A final remark concerns the target value for the relative error set at the beginning, i.e. 10%. As already discussed, the weight function method represents an approximation and a good match with the Monte Carlo simulation can be achieved only under the conditions discussed in section 4.3. We now focus on one poloidal LOS, CPF-07 at $R = 1.76$ m, which is affected by a relative error exceeding 20% for #39648. Figure 17 shows the superposition of the Monte Carlo spectrum and the intensities in the wavelength ranges [659, 660] nm, [660, 661] nm and [661, 662] nm, calculated using both the FIDASIM weight function method and the new fast method. The former slightly underestimates the Monte Carlo intensity, while the latter overestimates it. Both approaches show a relative error between 10% and 15% with respect to the Monte Carlo result. This highlights that a good agreement, i.e. within the target relative error, must be searched when a high compatibility between the Monte Carlo simulation and the weight function method is ensured.

The cause of the observed discrepancy between the fast method and FIDASIM in the poloidal lines of sight calculation has not been investigated further, since the work is focused on reproducing the intensity along the toroidal (CER) lines, which are showing a nice performance in each step of the work. The investigation and the improvement of the results in the other LOS will be part of future work.

## ORCID iDs

B Tosto 0009-0009-8621-8919
M Weiland 0000-0002-5819-9724
M Cavedon 0000-0002-0013-9753
A Kappatou 0000-0003-3341-1909
D Kulla 0000-0003-1621-7338

## References

[1] Heidbrink W W, Burrell K H, Luo Y, Pablant N A and Ruskov E 2004 Hydrogenic fast-ion diagnostic using balmer-alpha light *Plasma Phys. Control. Fusion* **46** 1855
[2] Hou Y M *et al* 2016 Fast-ion D$\alpha$ spectrum diagnostic in the EAST *Rev. Sci. Instrum.* **87** 11E552
[3] Muscatello C M, Heidbrink W W, Taussig D and Burrell K H 2010 Extended fast-ion D-alpha diagnostic on DIII-D *Rev. Sci. Instrum.* **81** 10D316
[4] Weiland M, Geiger B, Jacobsen A S, Reich M, Salewski M and Odstrčil T the ASDEX Upgrade Team 2016 Enhancement of the fida diagnostic at asdex upgrade for velocity space tomography *Plasma Phys. Control. Fusion* **58** 025012
[5] NIST 2026 Atomic spectra database (available at: https://physics.nist.gov/asd)
[6] Stagner L, Geiger B, and Heidbrink W FIDASIM: a neutral beam and fast-ion diagnostic modeling suite (https://doi.org/10.5281/zenodo.1341369)
[7] Geiger B *et al* 2020 Progress in modelling fast-ion d-alpha spectra and neutral particle analyzer fluxes using fidasim *Plasma Phys. Control. Fusion* **62** 105008
[8] Stagner L, Heidbrink W, Salewski M, Jacobsen A and Geiger B the DIII-D and A. U. Teams 2022 Orbit tomography of energetic particle distribution functions *Nucl. Fusion* **62** 026033

[9] Weiland M, Bilato R, Geiger B, Schneider P, Tardini G, Garcia-Muñoz M, Ryter F, Salewski M and H Zohm 2017 the ASDEX Upgrade Team and the EUROfusion MST1 team, Phase-space resolved measurement of 2nd harmonic ion cyclotron heating using fida tomography at the asdex upgrade tokamak *Nucl. Fusion* **57** 116058

[10] Stagner L and Heidbrink W W 2017 Action-angle formulation of generalized, orbit-based, fast-ion diagnostic weight functions *Phys. Plasmas* **24** 092505

[11] Salewski M *et al* 2014 On velocity-space sensitivity of fast-ion d-alpha spectroscopy *Plasma Phys. Control. Fusion* **56** 105005

[12] Kulla D, Lazerson S, Kappatou A, Weiland M and Wolf R the ASDEX Upgrade Team 2025 Validation of beams3d against fast-ion d-alpha measurements at asdex-upgrade using fidasim *Nucl. Fusion* **65** 086032

[13] Weiland M, Bilato R, Dux R, Geiger B, Lebschy A, Felici F, Fischer R, Rittich D and van Zeeland M 2018 the ASDEX Upgrade Team and the Eurofusion MST1 Team, Rabbit: real-time simulation of the nbi fast-ion distribution *Nucl. Fusion* **58** 082032

[14] Geiger B, Garcia-Munoz M, Heidbrink W W, McDermott R M, Tardini G, Dux R, Fischer R and Igochine V ASDEX Upgrade Team 2011 Fast-ion d-alpha measurements at asdex upgrade *Plasma Phys. Control. Fusion* **53** 065010

[15] Geiger B 2012 Fast-ion transport studies using fida spectroscopy at the asdex upgrade tokamak *PhD Dissertation* Ludwig-Maximilians-Universität München

[16] Lebschy A 2014 Electron density reconstruction using beam emission spectroscopy on a heating beam *Master's Thesis* Ludwig-Maximilians-Universität München (https://doi.org/10.1088/1741-4326/aabf0f)

[17] McDermott R M *et al* 2018 Evaluation of impurity densities from charge exchange recombination spectroscopy measurements at asdex upgrade *Plasma Phys. Control. Fusion* **60** 095007